

Supporting Information for

## Interfacial thermal resonance in an SiC–SiC nanogap with various atomic surface terminations

Xiangrui Li,<sup>‡a</sup> Wentao Chen,<sup>‡b</sup> and Gyoko Nagayama<sup>\*b</sup>

<sup>a</sup> Graduate School of Engineering, Kyushu Institute of Technology, Sensui 1-1, Tobata, Kitakyushu, Fukuoka 804-8550, Japan.

<sup>b</sup> Department of Mechanical Engineering, Kyushu Institute of Technology, Sensui 1-1, Tobata, Kitakyushu, Fukuoka 804-8550, Japan.

Email: nagayama.gyoko725@mail.kyutech.jp

### 1. Molecular dynamics simulation method

NEMD simulations of the SiC computational domain with a nanogap were carried out using Large-scale Atomic/Molecular Massively Parallel Simulator (LAMMPS). Fig. 1(b) shows the simulation system with the dimensions of  $L_x = 5.90$  nm,  $L_y = 5.90$  nm,  $L_z = 2.98$  nm, and the nanogap distance  $D$  between the separated solid walls was 0.436 nm (1 $a$ , where  $a$  is the lattice constant of 3C-SiC).<sup>1</sup> The heating or cooling wall consists of 5 layers of SiC diatomic molecules with its (111) plane facing the vacuum nanogap. The numbers of SiC molecules were 4180. It is possible to have different atomic surface terminations on 3C-SiC, such as Si termination and C termination, as shown in Fig. 1(c). Specifically, there are four pairs of atomic surface terminations (C–Si, Si–C, Si–Si, and C–C). In each case, the left and right side terms indicate the corresponding atomic surface terminations of the interfacial layers at the heating and cooling walls, respectively.

The Si–Si, Si–C, and C–C interactions for the SiC molecules were represented by the Vashishta potential with a cut-off distance of 0.735 nm.<sup>2-3</sup> Periodic boundary conditions were applied in the  $x$  and  $y$  directions for the simulation system. The outermost layers are the fixed layers, as well as the heating and cooling layers are controlled by Langevin thermostats with the constant temperature of 320 K and 280 K, respectively. A time step of 1 fs was set for all NEMD simulations. The simulation systems were initially run in the canonical ensemble (NVT) at 280 K for 6 ns. Subsequently, the NEMD simulations were performed for 10 ns to reach the steady state in the microcanonical ensemble (NVE).

The temperature of each solid layer was calculated for 20 ns data sampling in the steady NEMD simulations. The mean value of the net heat flux for the simulation system is calculated as

$$q = \frac{1}{A} \cdot \frac{\partial E}{\partial t}, \quad (1)$$

where  $A$  is the cross-sectional area of the simulation system in the  $x$ – $y$  plane,  $\partial E / \partial t$  is the heat transfer rate, and  $E$  is the cumulative energy input or output of the simulation system. The thermal gap conductance  $G$  between the interfacial layers in a nanogap is calculated as follows

$$G = \frac{q}{T_{\text{Hi}} - T_{\text{Ci}}}, \quad (2)$$

where  $T_{\text{Hi}}$  and  $T_{\text{Ci}}$  are the temperatures of interfacial layers at the heating and cooling walls, respectively.

The atomic vibrational displacements and frequencies were calculated using a wave graph to analyze the atomic vibrational characteristics.<sup>4-5</sup> Based on simulation data of 200 ps under steady state, the wave graph was obtained by signal analysis of original atomic positions. The equilibrium position of the atoms in the  $z$ -direction is calculated as

$$\bar{z} = \frac{1}{t_f - t_0} \sum_{t_0}^{t_f} z_{i,t}, \quad (3)$$

where  $z_{i,t}$  represents the position of atom  $i$  at time  $t$  in the  $z$ -direction,  $t_0$  and  $t_f$  are the initial time and extended finite time for data sampling of 40,000 time steps, respectively. Fig. 1(c) shows the location of Si and C atoms at the center of interfacial layers for calculating the atomic vibrational displacements. The original vibrational displacements of atom  $i$  are calculated as  $\Delta z_{i,t} = z_{i,t} - \bar{z}$ . Then, we calculate the Fourier transform of the original vibrational displacements to obtain the distribution of signal power in the frequency domain (power spectrum). The dominant frequency band is selected to perform signal filtering on the original vibrational displacements and obtain the regular wave graphs. The peak amplitude and frequency are determined from the wave graphs. Specifically, the strong phonon coupling at the interfacial layers leads to the resonant excitation peaks of the VDOSs in the frequency band coinciding with the dominant frequencies of the interfacial atoms.

The VDOS<sup>6-8</sup> of atomic terminated layers was calculated using all atomic velocities of the atomic terminated layers during 200 ps under steady state based on the Fourier transform of the velocity autocorrelation function:

$$\text{VDOS}(\omega) = \int_0^{\infty} \langle \vec{v}(t) \vec{v}(0) \rangle e^{-i\omega t} dt, \quad (4)$$

where  $\omega$  is the angular frequency, and  $v(t)$  is the atomic velocity at time  $t$ .

The normalized cross-correlation coefficient<sup>9</sup> between atomic vibrational displacements is calculated as:

$$r = \frac{\sum_{i=1}^n (x_i - \bar{x})(y_i - \bar{y})}{\sqrt{\sum_{i=1}^n (x_i - \bar{x})^2} \sqrt{\sum_{i=1}^n (y_i - \bar{y})^2}}, \quad (5)$$

where  $n$  is the sample size, and  $x_i, y_i$  are the displacements of two atoms in the  $z$ -direction abstracted from Fig. 4.  $\bar{x}, \bar{y}$  are the mean values of  $x_i, y_i$ .

The spectral heat current between atom  $i$  and  $j$  can be expressed as

$$Q_{ij}(\omega) = -\frac{2}{t_s \omega} \sum_{\alpha, \beta \in \{x, y, z\}} \text{Im} \langle \hat{v}_i^\alpha(\omega) * K_{ij}^{\alpha\beta} \hat{v}_j^\beta(\omega) \rangle, \quad (6)$$

where  $t_s$  and  $\omega$  are the simulation time and the frequency, respectively. “Im” denotes the imaginary part.  $\hat{v}_i^\alpha(\omega)$  and  $\hat{v}_j^\beta(\omega)$  are the Fourier transformed atomic velocities of atom  $i$  in direction  $\alpha$  and atom  $j$  in direction  $\beta$ , respectively, with “\*” representing the complex conjugate. The force constant matrix can be calculated as

$$K_{ij}^{\alpha\beta} = \frac{F_j^{\beta-} - F_j^{\beta+}}{2\Delta}. \quad (7)$$

Here,  $F_j^{\beta-}$  and  $F_j^{\beta+}$  denote the force on atom  $j$  in  $\beta$  direction when atom  $i$  is displaced to  $-\alpha$  and  $+\alpha$  directions, respectively. The phonon transmission function can be defined according to the spectral heat current

$$\Gamma(\omega) = \frac{Q(\omega)}{k_B \Delta T_i}, \quad (8)$$

where  $k_B$  is the Boltzmann constant and  $\Delta T_i$  is the temperature difference between the interfacial layers in NEMD simulations. The spectral thermal conductance per unit area is finally obtained as

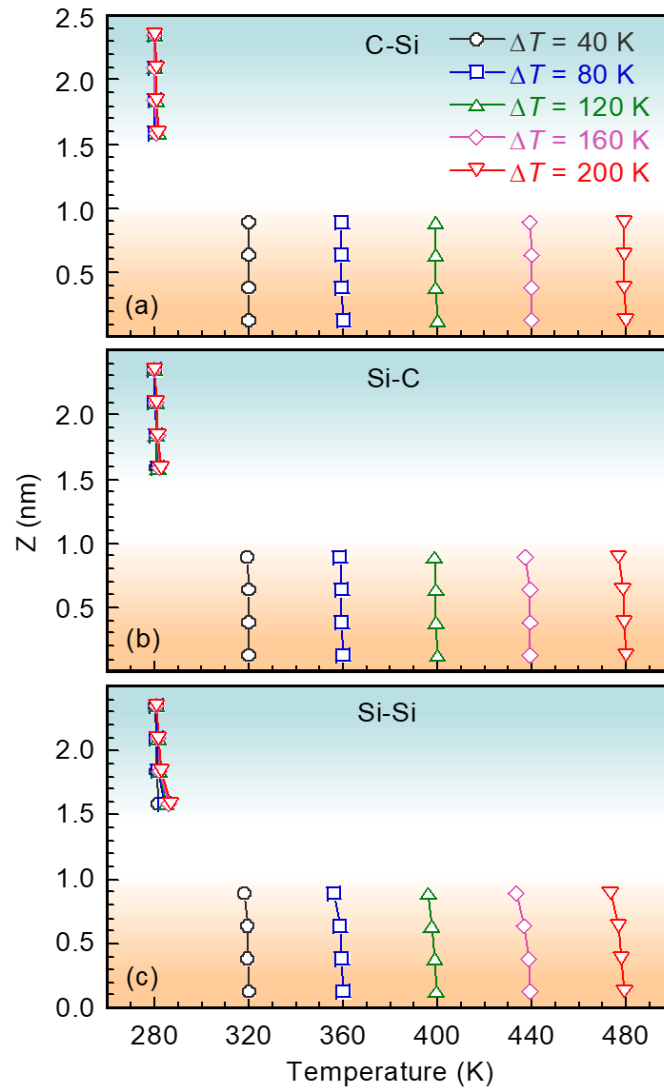
$$G(\omega) = \frac{Q(\omega)}{A \Delta T_i}, \quad (9)$$

where  $A$  is the  $x$ - $y$  cross-section area.

## 2. Temperature profiles under various $\Delta T$

The temperature profiles of solid walls for the nonidentical cases of C–Si, Si–C, and the identical case of Si–Si are shown in Fig. S1. Compared to the identical case of Si–Si,

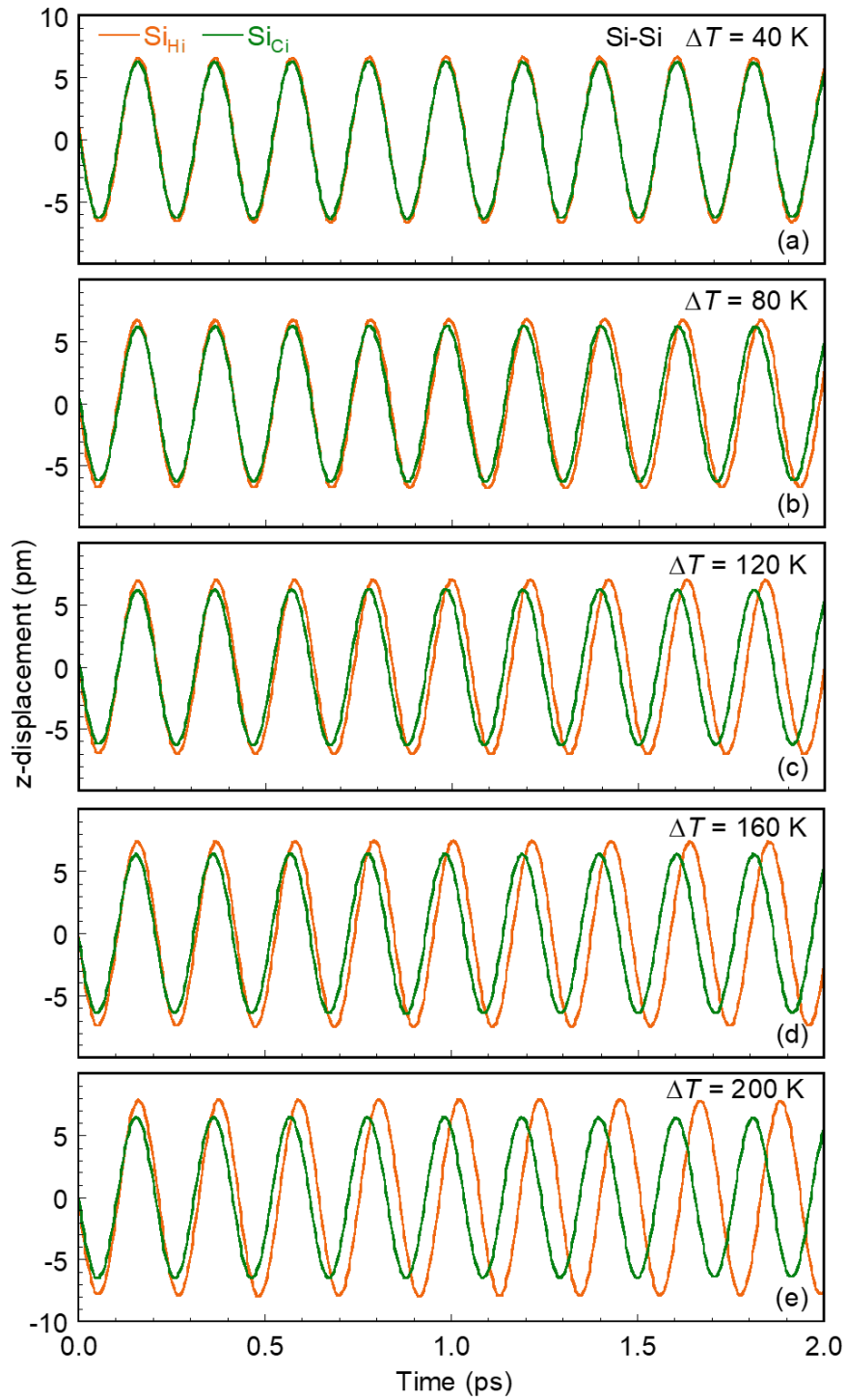
the temperature jump at the interfacial layers  $\Delta T_i (= T_{Hi}-T_{Ci})$  is nearly identical to  $\Delta T (= T_H-T_C)$  between the heating ( $T_H$ ) and cooling ( $T_C$ ) layers for the nonidentical cases of C-Si and Si-C. The temperature gradient of both heating and cooling walls increases with an increment in  $\Delta T$  for the identical case of Si-Si. The results further verified that atomic surface terminations can affect thermal energy transport across the vacuum nanogap.



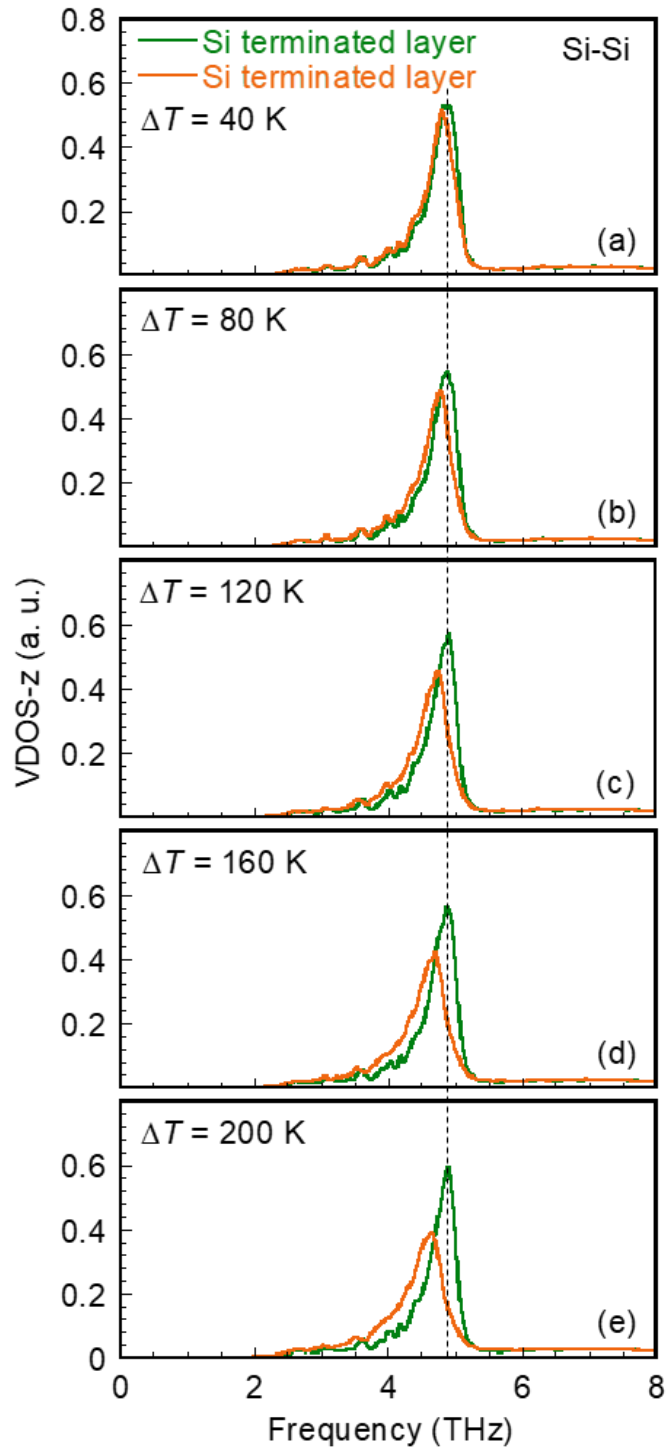
**Fig. S1** Temperature profiles of the solid walls in the steady NEMD simulations along the  $z$ -direction under various temperature difference  $\Delta T$  between heating and cooling layers with various atomic surface terminations: (a) C-Si, (b) Si-C, and (c) Si-Si.

### **3. Atomic vibrational displacements under various $\Delta T$**

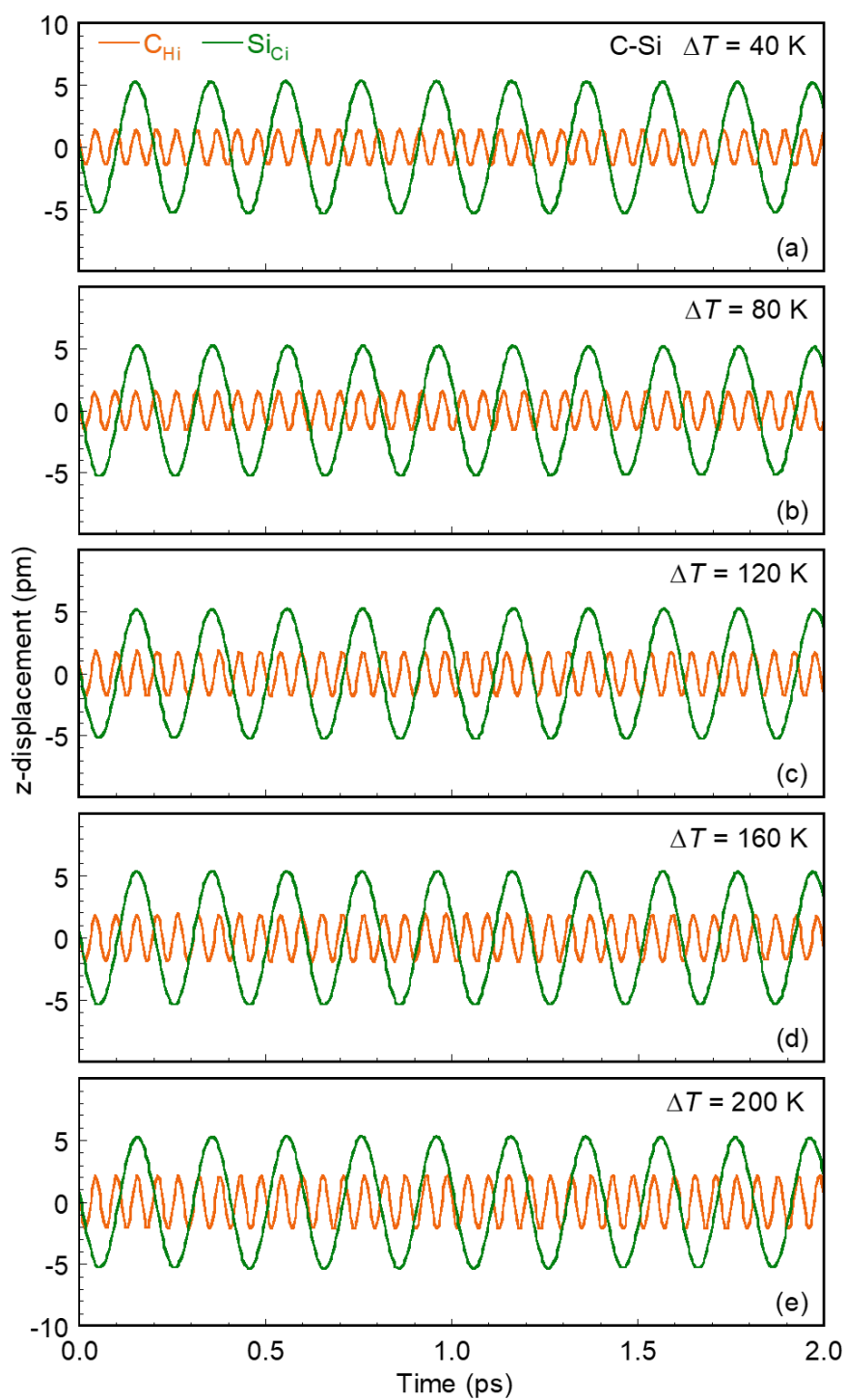
Atomic vibrational displacements of the heating and cooling interfacial layers in the identical case of Si–Si under various  $\Delta T$  between thermostats are shown in Fig. S2. The temperature at the heating interfacial layer  $T_{\text{Hi}}$  varies from 317.90 K to 473.23 K, resulting in an increase of atomic vibrational displacement with  $T_{\text{Hi}}$ . However, the atomic vibrational displacement at the cooling interfacial layer undergoes little changes because the temperature at the cooling interfacial layer varies extremely low (in a range of 281.46–286.67 K). Therefore, the mismatch of vibrational displacements for Si–Si between the heating and cooling interfacial layers is mainly caused by the temperature dependence of the atomic vibrational displacements.



**Fig. S2** Atomic vibrational displacements of the identical case of Si–Si in the heating and cooling interfacial layers under various temperature difference  $\Delta T$  between heating and cooling layers.



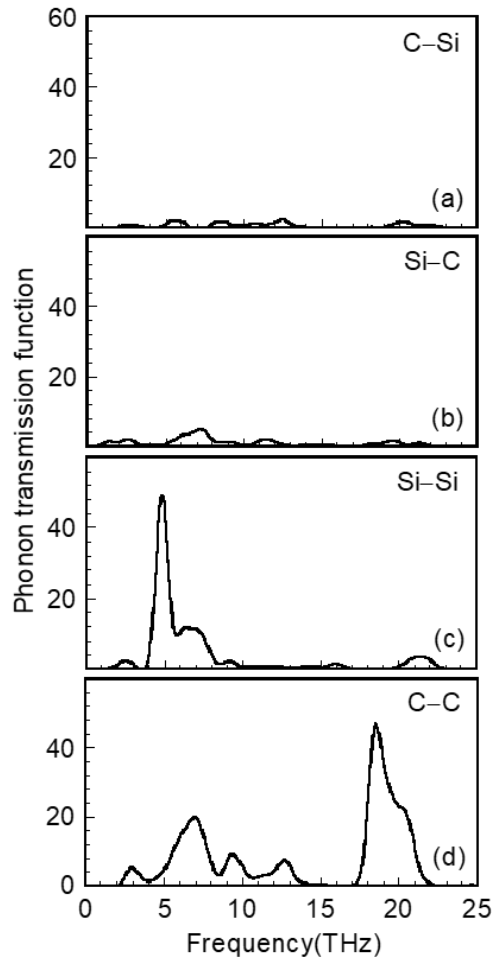
**Fig. S3** VDOSs in the  $z$  direction at atomic terminated layers of the identical case of Si-Si under various temperature difference  $\Delta T$  between heating and cooling layers.



**Fig. S4** Atomic vibrational displacements of the nonidentical case of C–Si in the heating and cooling interfacial layers under various temperature difference  $\Delta T$  between heating and cooling layers.

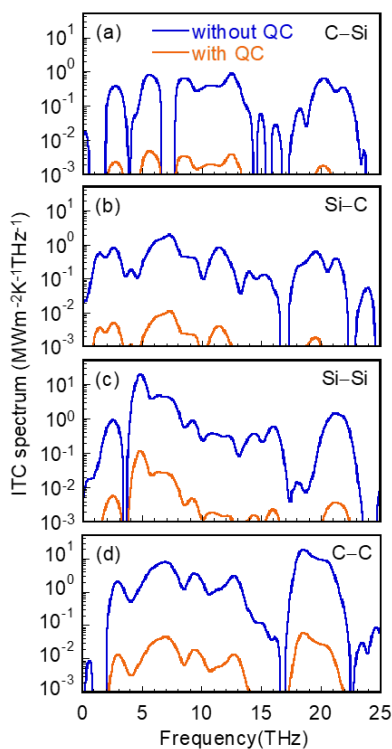
#### 4. Phonon transmission function

Fig. S5 shows the interfacial transmission coefficients for various atomic surface terminations. The results indicate that the interfacial transmission coefficients of the nonidentical cases are significantly lower than those of the identical cases. The lower interfacial transmission coefficient of the nonidentical cases can be attributed to the phonon mismatch between the heating and cooling interfacial layers, which can be verified in Fig. 5 (a) and (b). In the identical cases, the acoustic phonons are dominant for Si-Si (4–8 THz), whereas optical phonons are the primary heat carriers for C-C (18–22 THz).



**Fig. S5** Phonon transmission function  $\Gamma(\omega, T)$  for various atomic surface terminations: (a) C-Si; (b) Si-C; (c) Si-Si; (d) C-C.

## 5. Quantum effects on spectral thermal conductance



**Fig. S6** The spectral thermal conductance with (orange line) and without (blue line) quantum correction for atomic surface terminations: (a) C–Si; (b) Si–C; (c) Si–Si; (d) C–C. The vertical axis is in logarithmic scale.

### References

- 1 C.U. Gonzalez-Valle, S. Kumar and B. Ramos-Alvarado, *J. Phys. Chem. C.*, 2018, **122**, 7179–7186.
- 2 P.Vashishta, R. K. Kalia, A. Nakano and J. P. Rino, *J. Appl. Phys.*, 2007, **101**, 103515.
- 3 B. Yang, Q. Deng, Y. Su, X. Peng, C. Huang, A. Lee and N. Hu, *Comput. Mater. Sci.*, 2022, **203**, 111114.
- 4 W. Chen and G. Nagayama, *Int. J. Heat Mass Transf.*, 2021, **176**, 121431.
- 5 W. Chen and G. Nagayama, *Phys. Chem. Chem. Phys.*, 2022, **24**, 11758–11769.
- 6 H. Bao, J. Chen, X. Gu and B. Cao, *ES Energy Environ.*, 2018, **1**, 16–55.

- 7 X. Liu, D. Surblys, Y. Kawagoe, A. R. B. Saleman, H. Matsubara, G. Kikugawa and T. Ohara, *Int. J. Heat Mass Transf.*, 2020, **147**, 118949.
- 8 B. Wang, Z. Xu, X. Wang and W. Yan, *Int. J. Heat Mass Transfer.*, 2018, **125**, 756–760.
- 9 J. L. Rodgers and W. A. Nicewander, *Am. Stat.*, 1988, **42**, 59–66.